Parallel Computing of Thermo-Fluid Modeling Related to the FSW Process

Asdin Aoufi, Frank Montheillet, Christophe Desrayaud

▶ **To cite this version:**

Parallel computing of thermo-fluid modeling related to the FSW process

Asdin AOUFi[1,a],   , Frank MONTHEILLET[2,b],
Christophe DESRAYAUD[3,c]

[1,2,3]Mines Saint-etienne, Univ Lyon, CNRS, UMR 5307 LGF,
158 cours Fauriel Saint-Etienne,France.
[a]aoufi@emse.fr, [b] montheil@emse.fr, [c]cdesray@emse.fr

Abstract

This paper is devoted to the numerical computation of a steady-state thermo-fluid modeling related to the Friction Stir Welding Process in a two-dimensional cylindrical geometry. It analyzes the efficiency of the implementation on parallel architectures of two finite-difference schemes on a structured grid. The first one applies the Newton-Raphson method to compute a numerical solution of this non-linear elliptic type equation, and uses an iterative sparse solver. The second one is based on a time-marching approach converging to the steady state solution thanks to a time-explicit computation. Their respective performance is presented and discussed. Some numerical simulation results are presented to validate the proposed approach.

1   Introduction

A steady-state thermo-fluid modeling related to the Friction Stir Welding Process was provided by [1]. Its key feature is the velocity field used in the non-linear advection-reaction diffusion equation in 2D and 3D cylindrical geometry. Robin and Neumann type boundary conditions are required in this Eulerian formulation. The main numerical difficulties are related to the global velocity field describing the material flow around the tool in the advection term and the exothermic term taking into account the equivalent von Mises plastic strain rate. This non-linear elliptic type partial differential equation can be solved by a standard finite-difference numerical scheme on a structured grid, but it is known that special care is required to handle the advection term. The organization of the paper is the following. Section 2 summarizes the governing equations

of the modeling including the expression of the boundary conditions and the velocity field which takes into account the bulk material flow around the pin [2] and the circulation of the material around the pin to account for rotative dragging of the bulk material by the probe [1]. Section 3 describes the main features of the numerical schemes used to discretize both the steady state and the time dependent heat transfer equation. The handling of the advection term requires an upwind technique similar to the Petrov-Galerkin method developed in the finite-element approach to ensure stabilization of the numerical scheme. Section 4 analyzes the parallelization strategy on multi-core architectures using OpenMP and many-core architectures using CUDA of both numerical schemes. Section 5 presents the speedup obtained by both implementations. Finally several welding conditions are used to validate the numerical simulations results, after a careful grid refinement study was done. The spatial distribution of the computed temperature field is provided to show the effect of the welding velocity of the tool for a tool rotational velocity equal to 40 rpm but also as a function of the tool rotational velocity for a welding velocity equal to 1, 100 and 400 mm/s. A conclusion summarizes the results obtained in this study.

2 Mathematical modelling

The section presents the equations of the steady-state thermo-fluid modeling provided in [1],[2],[3]. The geometry is a section of a hollow cylinder by a plane orthogonal to the cylinder axis of symmetry. The internal radius is Ri [m] and the external radius is Re [m].

2.1 Governing equations

Thanks to the Eulerian steady state formulation of the enthalpy balance, the following partial differential equation expressed in conservation form

$$S + \nabla.(\lambda T) + \Gamma_d K e^{\left(\frac{mQ}{RT}\right)} \dot{\bar{\varepsilon}}^{m+1} = \rho C_p \mathbf{V}.\nabla T. \tag{1}$$

where λ is the thermal conductivity in [W.m-1.K-1], T is the temperature in [K], $\Gamma_d = 0.92$ is the Taylor-Quinney parameter taking into account the fact that only a small part of the energy is stored in the material in form of defects. K is the "viscosity like" parameter [MPa.sm], m is the strain rate sensitivity, Q is the activation energy of the material flow [kJ.mol-1], is the equivalent von Mises plasticstrainrate, ρ is the material density [kg.m-3],and Cp is the specific heat[J.kg-1.K-1]. The power injected is denoted by S.

2.2 Boundary condition

Eq.(2) gives the third order Robin type boundary condition on the internal surface of the tool pin (r=Ri), and on its external surface (r=Re) is characterized by the heat transfer coefficient H such that

$$-\lambda \frac{\partial T}{\partial n} = H \left(T - T_\infty \right). \tag{2}$$

2.3 Velocity field

The circumvective two-dimensional velocity field $\mathbf{V} = (v_r(r,\theta), v_\theta(r,\theta))$ describing the material flow around the pin is given in Eq. (3), Eq.(4) where r_0 is the pin radius, r is the distance to the tool axis, Γ [m2s-1] is the material circulation and v_∞ [m.s-1] is the welding velocity.

$$v_r(r,\theta) = v_\infty \left(1 - \left(\frac{r_i}{r} \right)^2 \right) \cos \theta \tag{3}$$

$$v_\theta(r,\theta) = -v_\infty \left(1 + \left(\frac{r_i}{r} \right)^2 \right) \sin \theta - \frac{\Gamma}{2\pi r}. \tag{4}$$

2.4 Equivalent von Mises strain rate $\dot{\bar{\varepsilon}}(r,\theta)$

The equivalent strain rate $\dot{\bar{\varepsilon}}(r,\theta)$ is calculated from the strain rate tensor thanks to Eq.(5).

$$\dot{\bar{\varepsilon}} = \dot{\bar{\varepsilon}}(r,\theta) = \sqrt{\frac{2}{3} \sum_{i,j} \epsilon_{i,j}^2} = \sqrt{\frac{4}{3} \left[\left(\frac{2r_i^2 v_\infty}{r^3} \right)^2 + \left(\frac{\Gamma_d}{2\pi r^2} \right)^2 - \frac{r_i^2 v_\infty \Gamma_d \sin(\theta)}{\pi r^5} \right]}. \tag{5}$$

3 Numerical discretisation scheme

This section details the main characteristics of the numerical schemes used to discretize Eq. (3). The first one requires to solve a succession of linear systems, while the second one advances the solution in time to converge towards the steady-state solution. It is worth mentioning that special care was used to take into account the angular periodicity of the solution in the implementation. Several validation tests were done to validate the numerical scheme and the implementation.

3.1 Discretization of the steady state heat equation

A finite-difference discretization with an upwind technique for handling the advection term similar to the Petrov-Galerkin method is used. At each grid point, the local Peclet is computed to monitor the local numerical diffusion of the first-order scheme. In order to reduce this numerical diffusion, the grid is sufficiently refined in both r and θ directions. This five points stencil leads to the matrix formulation of the form $A(T)T = b(T)$, where A is a sparse periodic pentadiagonal matrix, i.e. periodic block-tridiagonal matrix. T is the vector of all unknowns and $b(T)$ is a vector taking into account the exothermic term $\Gamma_d K e^{\left(\frac{mQ}{RT} \right)}$. The Newton-Raphson iterative method is used to obtain the solution of the non-linear system. The tangent matrix arising at each step is non-symmetric.

3

A simple iterative procedure is used to solve the linear system at each step, and converges quickly due to the mathematical properties of this tangent matrix.

3.2 Discretization of the boundary conditions

A two-points, first order finite-difference approximation of the two Robin type boundary conditions was used. It was proved mathematically that the temperature computed at these grid points fulfills a discrete maximum principle.

3.3 Discretization of the unsteady heat equation

A simple time-explicit finite-difference scheme was used to handle the non-linear advection-reaction-diffusion equation. A stability condition over the time-step was rigorously established, in order to ensure the positivity i.e. a discrete maximum principle for the numerical solution and was taking into account the thermal conductivity, heat capacity, mass density, components of the velocity field and mesh size. No sparse solver was needed at each step, this was a main advantage over an implicit discretization scheme, even if the admissible time-step was constrained by a stability condition.

4 Parallelization strategy

The two numerical schemes were implemented in C, on an Intel i7-8750H, 6 cores cpu and parallelized thanks to inserting OpenMP pragma [6] and on an NVIDIA QUADRO P3200 gpu having 1792 shading units using CUDA [7] kernels. An analysis of the computational complexity of the numerical scheme was done in order to quantify the throughput of the code on these two parallel architectures. We focus, on the time-explicit implementation for which the speed-up are significant after validating the computed solution after convergence to the steady state regime with the one computed by the Newton-Raphson method. On a 80x184 structured finite difference grid, the speedup obtained versus one cpu core for 105 time-steps using OpenMP is 7 when using 12 cores and above 30 when using CUDA. Further improvements of the performance obtained by the CUDA implementation are currently investigated. We conclude that using such programming paradigm is quite efficient to simulate this advection-reaction-diffusion time dependent equation using a simple time explicit scheme.

5 Results and discussion

5.1 Circumvective velocity field and Equivalent von Mises strain rate

For a tool rotational velocity of 40 rpm, we investigate the effect of the welding velocity equal to 1, and 400 mm/s of both 2D fields represented in Fig.(1).
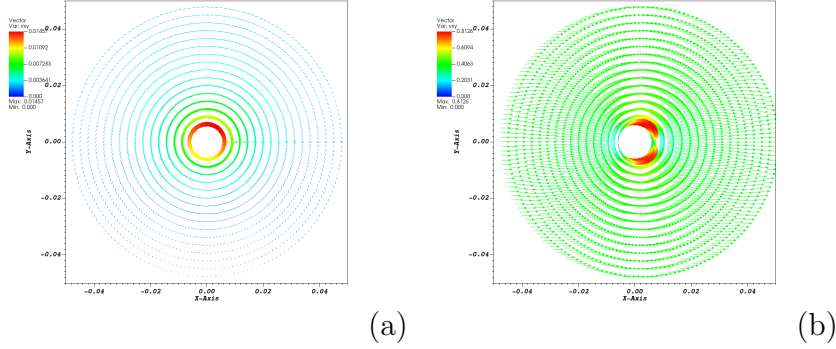
Figure 1: Circumvective velocity field for a tool rotational velocity of 40 rpm, we investigate the effect of the welding velocity equal to 1, and 400 mm/s.

The symmetry of both fields is observed, moreover the intensity is maximum near the boundary $r = Ri$ due to Eq.(3) and Eq.(4).

5.2 Equivalent von Mises strain rate field

Fig.(2) shows that the shape is similar, even if the intensity is multiplied by 75 when the tool velocity is multiplied by 400 and the highest value is located near $r = Ri$.
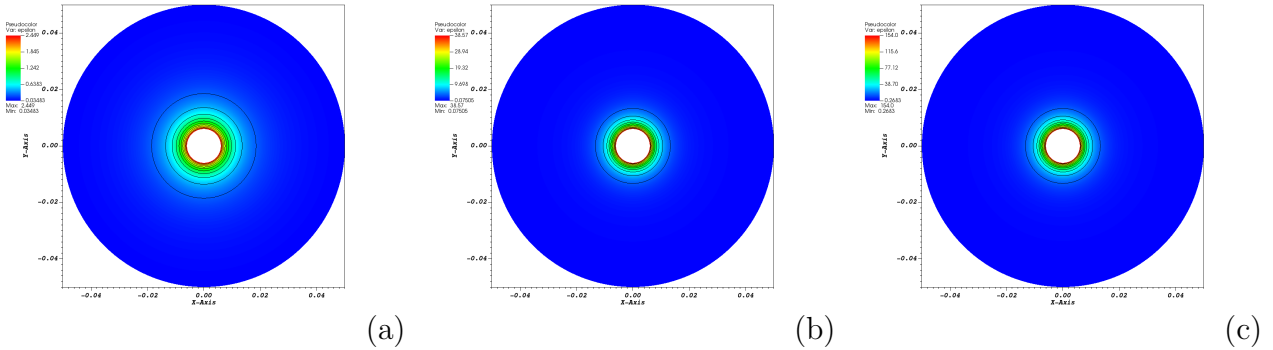

Figure 2: Equivalent von Mises strain rate field, for a tool rotational velocity of 40 rpm, we investigate the effect of the welding velocity equal to 1, 100 mm/s and 400 mm/s.

5.3 Numerical simulation results

Fig.(3) shows that the temperature increase is quite moderate even when the welding velocity is high (case (a), (b) and (c)). We observe that temperature field is similar in shape for high value of

5

the welding velocity. When the welding velocity is small, the modeling reduces to a simple linear heat equation in a cylindrical coordinate, so the iso-temperature curves are circles. The modeling could be therefore one-dimensional only. Finally, The maximum of the temperature is obtained near r=Ri, i.e; when the heat released is the highest but it doesn't match to the values obtained in [1],[3].

So we add a power injection S to feature the power injected by the shoulder friction on the top of the metal sheet to provide a more realistic modeling.

We point out that the top tool friction power (shoulder friction) does not stand in the 2D model due to the geometric simplification. As seen in Fig.(3)(d). We have added a uniform constant density located in the domain Ri¡=r¡=Rc, where Rc=15mm. In this case Fig.(3)(d), the tuning of the parameter S leads to more realistic temperature distribution, with a notable increase of the temperature. Further simulations are required to validate the approach.
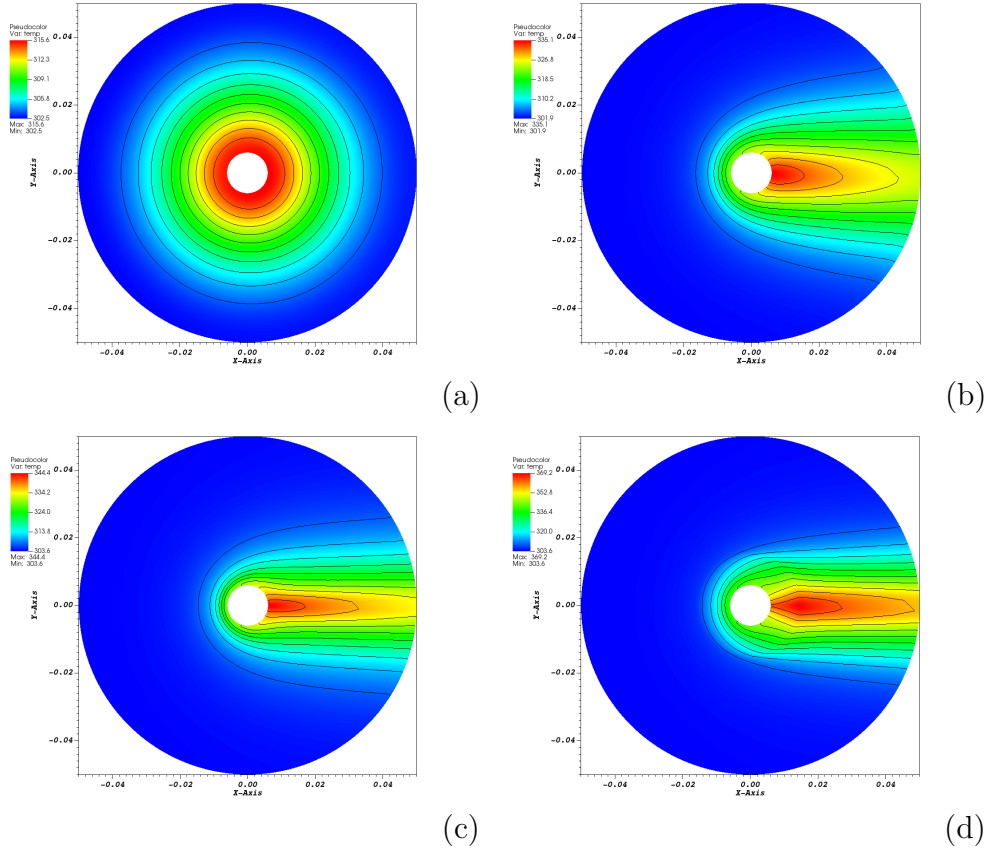

(a) (b)

(c) (d)

Figure 3: Steady-state temperature distribution obtained for a welding velocity of 1mm/s (a), 100 mm/s (b) and 400 mm/s (c) and (d) (power injection S in J/m^3 on domain $Ri <= r <= Rc$).

6

6   Conclusions and perspectives

In the present paper, we have analyzed how the welding velocity contributes to the temperature field thanks to the parallel implementation using CUDA on a gpu of a simple time-explicit finite-difference scheme on a structured uniform grid in a 2D polar coordinate system. A speed-up greater than 30 was obtained versus one cpu core. A more realistic modeling is genuinely three-dimensional. For this very reason, a similar study is currently under development for the 3D steady state modeling presented in [1]. Moreover in order to fully validate the discretization of the advection term, a second order upwind scheme will be also implemented, to compare the accuracy of both numerical solutions.

References

[1] D.Jacquin,C.Desrayaud,F.Montheillet, Mat.Sci.Forum 539-543 (2007) 3832-3837.

[2] P. Heurtier, M.J. Jones, C. Desrayaud, J.H. Driver, F. Montheillet, D. Allehaux, Journal of Materials Processing Technology 171 (2006) 348-357.

[3] D. Jacquin, B. de Meester, A. Simar, D. Deloison, F. Montheillet, C. Desrayaud, Journal of Materials Processing Technology 211 (2011) 57-65.

[4] D. Jacquin, B. de Meester, A. Simar, D. Deloison, F. Montheillet, C. Desrayaud, Science and Technology of Welding and Joining 9 (2004) 483-492.

[5] O.Grong, Metallurgical Modelling of Welding, second ed., The Institute of Materials, London, 1994.

[6] B. Chapman, G. Jost, R. Van De Pas, Using OpenMP-Portable Shared Memory Parallel Programming, MIT Press, Cambrige, 2007.

[7] J. Sanders, E. Kandrot, CUDA by Example: An introduction to General-Purpose GPU Programming, Addison-Wesley Professional, Boston, 2010.